Symmetry-breaking-induced off-resonance second-harmonic generation enhancement in asymmetric plasmonic nanoparticle dimers

Yaorong Wang, Zhiwei Peng, Yannick De Wilde, Dangyuan Lei

▶ **To cite this version:**

Yaorong Wang, Zhiwei Peng, Yannick De Wilde, Dangyuan Lei. Symmetry-breaking-induced off-resonance second-harmonic generation enhancement in asymmetric plasmonic nanoparticle dimers. Nanophotonics, 2024, 13 (18), pp.3337-3346. 10.1515/nanoph-2024-0118 . hal-04787574

HAL Id: hal-04787574
https://hal.science/hal-04787574v1

Submitted on 17 Nov 2024

HAL is a multi-disciplinary open access archive for the deposit and dissemination of scientific research documents, whether they are published or not. The documents may come from teaching and research institutions in France or abroad, or from public or private research centers.

L'archive ouverte pluridisciplinaire **HAL**, est destinée au dépôt et à la diffusion de documents scientifiques de niveau recherche, publiés ou non, émanant des établissements d'enseignement et de recherche français ou étrangers, des laboratoires publics ou privés.

Symmetry Breaking-induced Enhancement of Second Harmonic Generation in Gold Nanosphere Dimers

Yaorong Wang,[†] Zhiwei Peng,[†] Yannick De Wilde,[‡] and Dangyuan Lei[,†]*

[†]Department of Materials Science and Engineering, City University of Hong Kong, 83 Tat Chee Avenue, Kowloon, Hong Kong S.A.R.

[‡]Institut Langevin, ESPCI Paris, CNRS, Université PSL, Paris, 75005 France

*E-mail: dangylei@cityu.edu.hk

ABSTRACT: The linear and nonlinear optical properties of metallic nanoparticles have attracted considerable experimental and theoretical research interest. To date, researchers have primarily focused on utilizing the large electromagnetic field enhancement associated with nanoparticle plasmon and investigated many potential applications. Among numerous nanoparticle structures, nanoparticle dimers, being a structurally simple and easy-to-prepare system, hold significant importance in the field of nanoplasmonics. In highly symmetric plasmonic nanostructures, although the second-order nonlinearity of the metal surface will be improved because of the enhanced plasmonic field, even-order nonlinear optical processes such as second harmonic generation (SHG) will still be quenched and thus optically forbidden. Under this premise, it is imperative to introduce geometric symmetry breaking. Here, we prepared a series of dimer composed of two nanospheres with different sizes and subsequently investigate the symmetry

breaking-induced effect on their nonlinear response. Our results demonstrate that under off-resonant excitation, the SHG intensities of gold nanosphere dimers can be significantly enhanced by symmetry breaking. However, under resonant excitation, near-field enhancement still mainly affects SHG. Therefore, in the design of novel plasmonic nanostructure with enhanced nonlinear optical properties, symmetry breaking will play an indispensable role.

KEYWORDS: Second-Harmonic Generation, Gold nanosphere dimer, Symmetry breaking, plasmon hybridization, nonlinear plasmonics

INTRODUCTION

In the past decades, plasmonic metal nanoparticles have attracted widespread attention due to their potential applications in catalysis, clinical diagnostics, optical data storage, etc.[1–6] Among different nanostructures, nanoparticle dimers composed of two nanospheres are promising candidates for generating huge electromagnetic fields in their gap region.[7-9] The nanosphere dimers possess rich plasmonic properties and are easy to fabricate, which makes them an appropriate platform for studying linear and nonlinear optical phenomena. Furthermore, the plasmonic modes of the dimer originate from the near-field interaction between the strongly localized surface plasmon resonance (LSPR) of each nanosphere, which can be modulated easily and efficiently by modifying the nanosphere size or gap distance.[10]

The tightly confined local electromagnetic field in the gap of nanosphere dimer promotes nonlinear optical effects such as SHG, which makes them a great platform to study and control the light-light interaction at nanoscale.[11–16] The radiation at the double frequency 2ω is produced by the nonlinear polarization P(2ω) generated by the interaction between the fundamental electric field E(ω) and medium. Two photons at the fundamental frequency ω are converted into one photon at second harmonic (SH) frequency 2ω, which can be described as[17,18]

$$\boldsymbol{P}(2\omega) = \chi^{(2)}\boldsymbol{E}(\omega)\boldsymbol{E}(\omega) \quad (1)$$

where $\chi^{(2)}$ is the second-order nonlinear susceptibility tensor. Similarly, we have

$$-\boldsymbol{P}(2\omega) = \chi^{(2)}(-\boldsymbol{E}(\omega))(-\boldsymbol{E}(\omega)) = \chi^{(2)}\boldsymbol{E}(\omega)\boldsymbol{E}(\omega) \quad (2)$$

From the above two equations, it can be seen that the SHG emission is forbidden in the centrosymmetric medium.

The research on metal dimers mainly focuses on plasmonic nanoparticles made of gold, silver, and copper. SHG is forbidden in their bulk counterparts because of the centrosymmetric arrangements of their atoms. As such, observed SHG signals are ascribed to (1) surface dipolar susceptibility, and (2) bulk quadrupole contribution originating in the retardation effect.[19,20] Generally, SHG output of metallic nanoparticles is highly sensitive to both shape and size. The nonlinear-optical conversion efficiency can be significantly impacted by shape imperfections that introduced local symmetry breaking,[21,22]potentially leading to the enhanced SHG emissions.[23] Therefore, nanoparticles made of non-centrosymmetric material demonstrate efficient SHG[24] which can be used for nonlinear optical microscopy,[25] nonlinear phase control[26] and sensing.[27]

In symmetric gold nanoparticle dimers, though LSPR strongly enhance local electric fields and thus nonlinear polarization in the near field,[16,28] the far-field SHG emission is limited by the structural symmetry of the dimers. However, once the symmetry is broken, the cancellation is incomplete resulting in the generation of SH light.[29–31] In this work, we analyze the SHG originating in the geometric symmetry breaking in Au nanosphere dimers in both off- and on-resonant conditions. Employing nonlinear microscopy of single dimer allows us to study the impact of gradual increase of the asymmetry on the far-field SHG intensity. We focus on individual nanosphere dimers rather than regular arrays, thereby eliminating any potential influence arising from collective effects, such as plasmonic surface lattice resonance (SLR) and other analogous phenomena.[32] We outline symmetry breaking and plasmon-driven field enhancement as two

principal mechanisms responsible for the observed SHG increase with the dimer asymmetry. Although the near-field enhancement still dominates the SHG emission under the on-resonant excitation condition, the SHG intensities of the Au nanoparticle dimers can be enhanced by the symmetry breaking under the off-resonant condition.

RESULTS AND DISCUSSION

The dimers used in this paper are prepared on Si/SiO_2 substrates, which are connected by alkanedithiol.[10,33–35] The advantage of Au-S bonds to realize dimer assembly is that the gap distance is stably controlled and homogeneous (see section S1). Figure 1(a)-(d) shows the geometry of the prepared gold nanodimer. The degree of asymmetry of dimer is defined by $\delta = |d_1 - d_2|/(d_1 + d_2)$. All dimers are assembled from 60 nm, 80 nm, and 100 nm diameter gold spheres with degrees of δ=0, 0.11, 0.14, and 0.25 (color-coded red, blue, orange, and green, respectively). Figure 1(e)-(h) show the measured dark-field (DF) scattering spectra of individual dimers with different symmetries under unpolarized excitation. A single stronger peak originating from the longitudinal bonding dipolar plasmon (LBDP) mode occurs between 700 nm and 800 nm, varying with the structural parameters of dimers.[36] The dimer's DF images and scanning electron microscopy (SEM) images were also shown alongside the DF spectra to better illustrate the scattering pattern and morphology of the nanosphere dimer with different symmetries. We specify the resonant wavelength of LBDP mode on the scattering spectra obtained from experiments with the error bar obtained from multiple measurements (see section S1). Single-particle optical characterization allowed us to exclude monomers and randomly formed oligomers from the target dimers (Figure S3(b) in Supporting Information).[37]

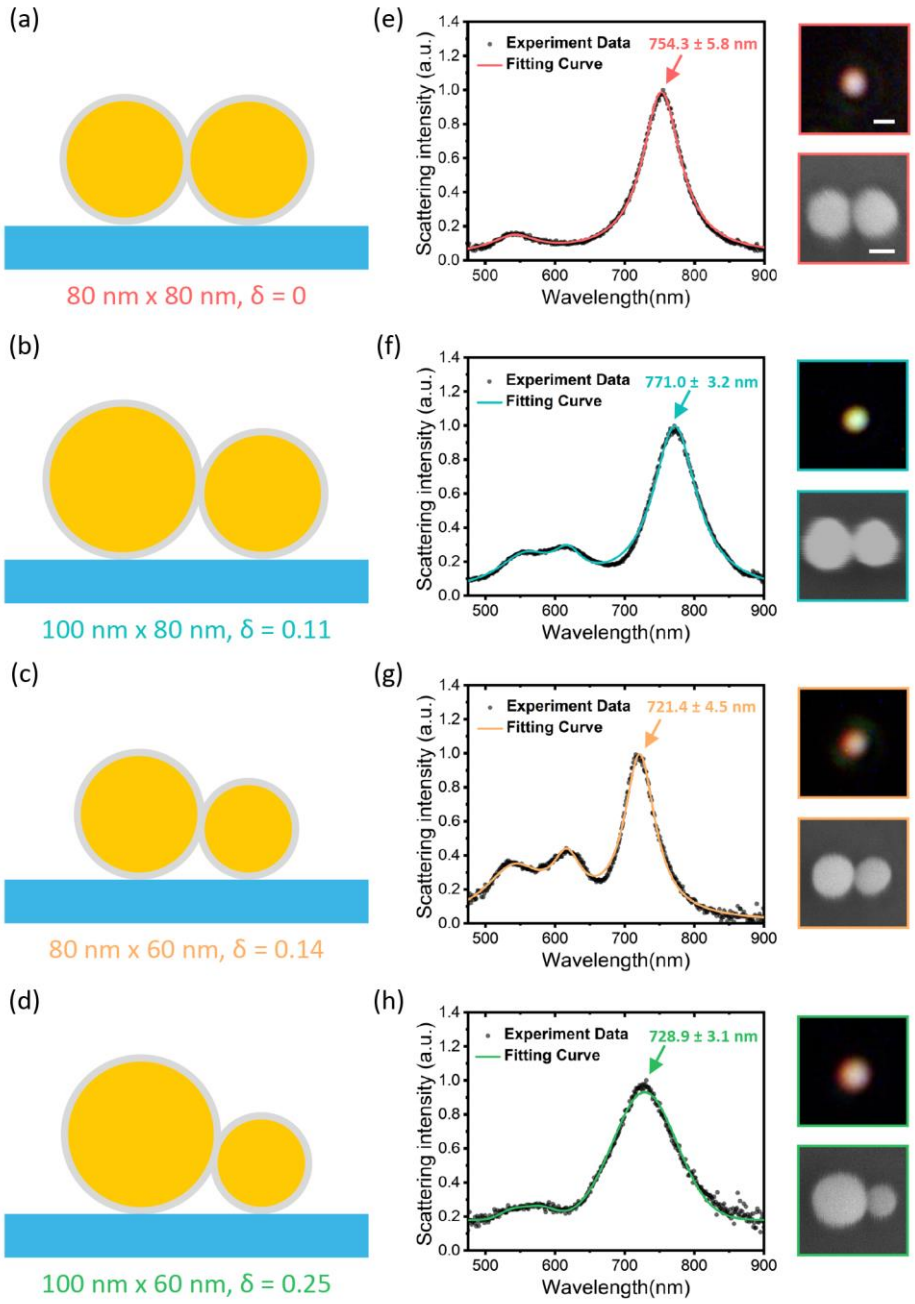

Figure 1. Optical linear properties of dimers with different degrees of asymmetry. (a–d) Schematic illustrations of fabricated symmetric and asymmetric dimers, where the diameters of the two spheres and their degree of asymmetry δ are labeled. (e-h) Measured DF scattering spectra of dimers with different degrees of asymmetry, where the peak position of LBDP mode and its error are marked. The solid lines are Lorentz fits to the scattering spectra (black dots). The scale bars in the DF image are 500 nm, and in the SEM image are 50 nm.

To better understand the nature of the modes of scattering peaks of the dimer, we further analyzed the plasmon hybridization modes by adding a polarizer in the collection optical path. (Figure S3(a) in Supporting Information) It is generally accepted that plasmon coupling can be considered analogous to molecular hybridization.[38,39] The dimer plasmons can be regarded as a combination of bonding and anti-bonding, that is, as a hybridization of single nanoparticle plasmons. The plasma modes of the two particles in the dimer (Ψ_1 and Ψ_2) can hybridize either in-phase ($\Psi_1 + \Psi_2$) or out-of-phase ($\Psi_1 - \Psi_2$). When the optical field is polarized along the inter-particle axis, i.e. longitudinal polarization, the in phase hybridization mode reflects the bonding mode (denoted as σ), the electric field in the gap of the dimer is enhanced, and the LSPR frequency is red-shifted. The out-of-phase hybridization mode is the anti-bonding mode (denoted as σ^*), with the electric field along the short axis of the dimer and a blue-shifted LSPR frequency.[40] Conversely, when the polarization is along the short axis of the dimer, i.e. transverse polarization, the in-phase hybridization mode is an anti-bonding mode (π^*), while the out-of-phase hybridization mode represents the bonding mode (π).

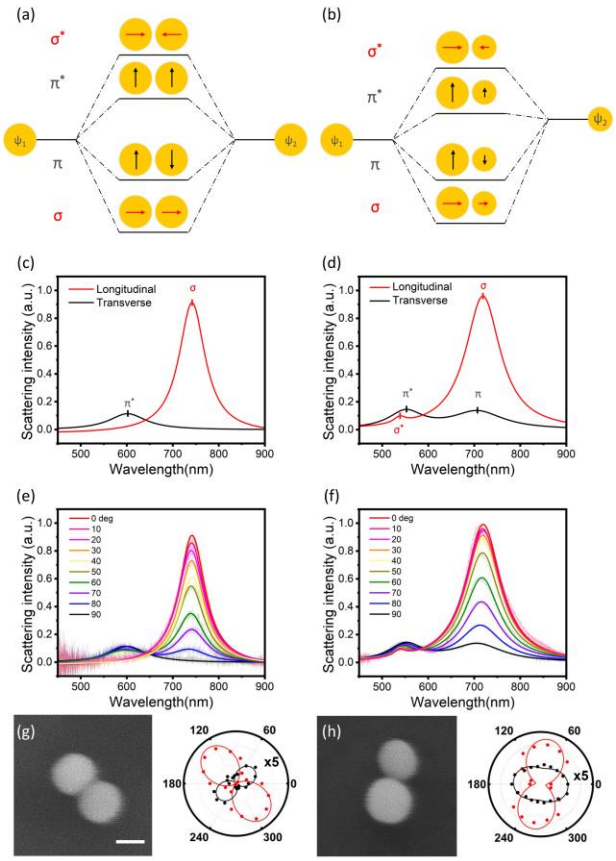

Figure 2. Different linear optical properties of symmetric and asymmetric gold nanoparticle dimer. hybridization model of symmetric (a) and asymmetric (b) dimer. (c) Transverse (black line) and longitudinal (red line) coupled mode of a symmetric gold nanoparticle dimer, where the in-phase mode is the only bright mode that can be optically detected in the far field. In contrast, an active out-of-phase mode is observed in the asymmetric dimer (d). Spectrums are derived from Lorentz fitting of experimental data. Scattering spectra of symmetric (e) and asymmetric (f) gold nanoparticle dimer at intermediate polarization angles between longitudinal mode (0°) and transverse mode (90°). The more transparent lines in the background are experiment data, and clearer curves are obtained by Lorentz fitting. Measured (dots) and fitted (line) polar plots of polarization-resolved scattering spectrum of symmetric (g) and asymmetric (h) dimer, in good agreement with the SEM figures. The scale bar is 50 nm. The transverse mode (black) is enlarged by 5 times for display.

Figure 2(a) and Figure 2(b) demonstrate the typical plasmon hybridization models of symmetric (80 nm x 80 nm) and asymmetric (80 nm x 60 nm) gold nanosphere dimers in this work. Consistent with the predictions of the plasmonic hybridization model, the scattering spectra of the symmetric dimers show two distinct modes. By rotating the polarizer in the collection optical path, the scattering spectra of the longitudinal and transverse polarization can be obtained. The Lorentz fitting curves of experimental results for these two cases are plotted in Figure 2(c). It can be seen that, whether it is longitudinal or transverse coupling, only the in-phase mode is optically allowed. In all intermediate angular orientations, the scattering spectrum is a linear combination of the two orthogonal modes,[41] shown in Figure 2(e) as a function of the polarizer angle. Although it is not possible in optical scattering experiments to independently know the angle of the polarizer relative to the inter-particle axis, we were able to assign the two modes through theoretical analysis.[39] Please note that in order to demonstrate the difference between symmetrical and asymmetrical dimers, here we uniformly set the inter-particle axis to 0 degrees instead of the real reading of the polarizer.

Likewise, Figure 2(d) shows the scattering spectra of longitudinal and transverse polarization of the asymmetric dimer. Both spectra contain two modes. This observation contrasts with the symmetric dimer, as expected according to the plasma hybridization model shown in Figure 2(b). The in-phase hybridization ($\Psi_1 + \Psi_2$) and the out-of-phase hybridization ($\Psi_1 - \Psi_2$) can be observed simultaneously, regardless of the longitudinal and transverse polarizations. That is, σ^* and π, which are dark in symmetric dimers, are active in asymmetric dimers, because of incomplete cancellation of the dipoles of the two different size particles.[42] Of course, in the weak coupling regime, the intensity of the out-of-phase mode will be much weaker than that of the in-phase mode. Similarly,

Figure 2(f) shows the scattering spectra of asymmetric dimer at intermediate angles between longitudinal and transverse polarizations.

The intensity of the scattering at the LSPR wavelength changes when rotating the polarizer, allowing us to determine the exact orientation of the dimer. In Figure 2(g)and (h), the scattering intensities of the bonding mode (red) and anti-bonding mode (black) of the symmetric and asymmetric dimers are shown as a function of polarization angle in polar coordinates. In good agreement with the SEM characterization, it exhibits a maximum at an axis angle of about ~130° for the symmetric dimer and about ~80° for the asymmetric dimer due to their respective longitudinal bonding dipolar plasmon (LBDP) mode along the dimer axis.[41,43,44] The transverse anti-bonding dipolar plasmon (TADP) mode, perpendicular to the dimer axis, is magnified five times for ease of display. The typical dipole-like pattern observed in experiments can be fitted by the cosine-square function, as shown by the dots and lines in Figure 2(g)and (h). The parameter called degree of polarization (DoP) defined as

$$DoP = \frac{I_{max} - I_{min}}{I_{max} + I_{min}} \tag{3}$$

can be used to quantitatively describe the dipole-like pattern polarization, where I_{max} (I_{min}) is the maximum (minimum) intensity parallel (perpendicular) to the dipole axis. In our case, a stronger linear polarization response was observed for the symmetric dimer (δ=0, DoP of 0.8 and 0.97 for TADP and LBDP, respectively) than for the asymmetrical dimer (δ=0.14, DoP of 0.27 for TADP and 0.76 for LBDP). Furthermore, as the δ continued to increase, a decrease in the DoP was observed (δ = 0.25, the DoP of TADP is 0.39, and the DoP of LBDP is 0.68). The noticeable reduction of DoP in asymmetric dimers indicates the non-negligible coupling between the plasmon modes. Originating in the geometric symmetry breaking, this coupling can be a fingerprint of the

mode hybridization, modulating the distribution of the electric field in the gap. In turn, the latter is key for the asymmetry driven SHG response of the nanosphere dimers, as we discuss below.

In order to qualitatively understand the modulation mechanism of symmetry breaking on the SHG, we have theoretically analyzed nanosphere dimers with different symmetries. As shown in the schematic diagrams of Figure 3(a)-(d), the dimer consists of two gold nanoparticles with a gap distance of 1.3 nm determined by monolayer dithiol.[35] The permittivity, similar to that of polyethylene, is approximately 2.25.[45–49] The simulations are based on a phenomenological free electron model. (see section S2) The fundamental light polarized along the main dimer axis excites the LBDP mode. For centrosymmetric metals, the main component of the nonlinear susceptibility tensor originates from the metal surface and is directed perpendicularly outwards.[50]

For the SHG of the symmetric dimer shown in Figure 3(a), the SH dipole moments are equal but opposite in direction. So the far-field radiation SHG is quenched by the destructive interference of the opposite dipoles, as shown in Figure 3(i) and (m). In the case of several asymmetric dimers shown in Figure 3(b)-(d), the SH dipole moments still demonstrate an anti-bonding distribution, but the structural asymmetry results in their imbalance leading to the non-vanishing far-field SHG output. The fundamental frequency field (Figure 3(e)-(h)) is driven by an incident plane wave, resulting in the field enhancement inside the gap. The SH field (Figure 3(m)-(p)) is driven by nonlinear polarization source at the metal surface.[51] Symmetry breaking in an asymmetric dimer occurs through two aspects: (1) local SHG polarization ($P^{0}_{z,2\omega}$ in Figure 3(j)-(l)) has an asymmetric distribution on the surface. (2) global SHG polarization ($P^{LSP}_{z,2\omega}$ in Figure 3(n)-(p)). Because of the larger surface area, the nonlinear polarization is always stronger on larger spheres than on smaller ones.

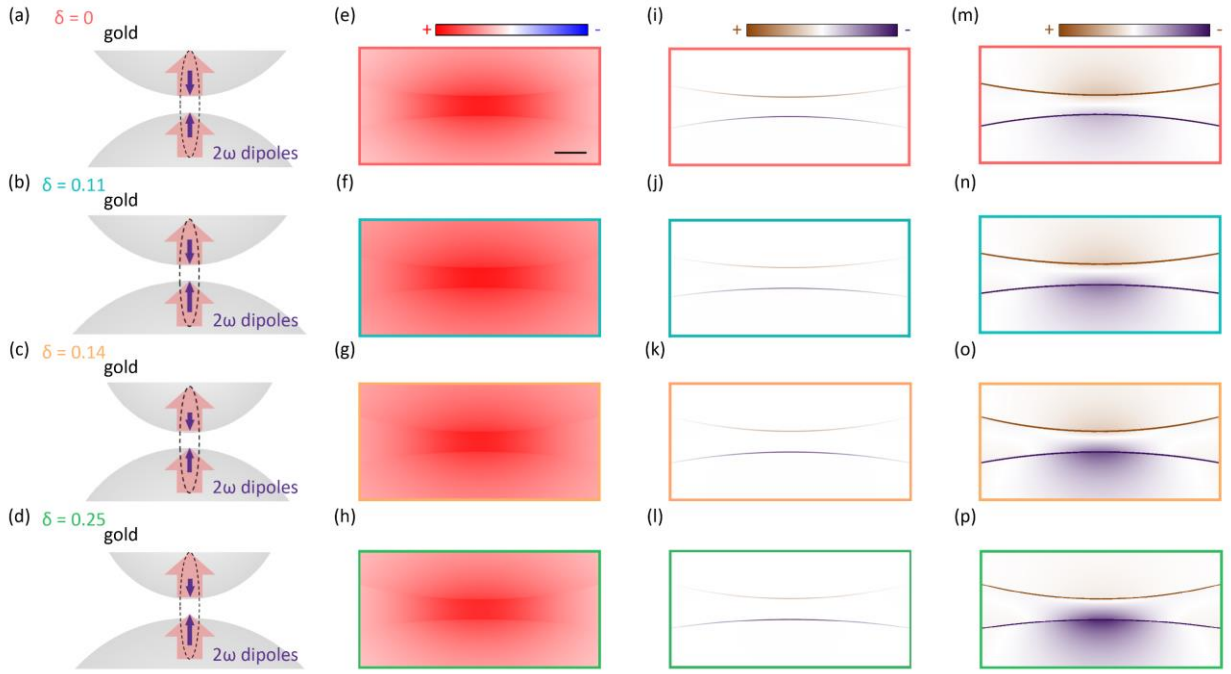

Figure 3. Analysis of the SH origin in gold nanosphere dimers with different symmetry conditions. (a)–(d) Schematics of the SH origin in the nanosphere dimers with varying degrees of asymmetry δ. Red thick arrows indicate the dipolar response to the driving field oriented along the nanogap, $E_{\perp}$. Purple arrows represent the induced 2ω dipoles responsible for the far-field SH radiation. (e)–(h) Simulated near-field polarization distributions, $P_{z,2\omega}$, at the fundamental wavelength of 900 nm for the structures in (a)–(d) with a gap g = 1.3 nm. Scale bar in (e) is 2 nm. (i)–(l) Calculated near-field polarization distributions, $P^{0}_{z,2\omega}$, at the SH wavelength induced by the respective fundamental fields (Eq. (1)), which are significant only at the interface of the centrosymmetric metal. (m)–(p) SH polarization distributions resulting from the non-resonant plasmonic coupling of the surface nonlinear sources in (i)-(l) to the dimers.

In our experiments, the output from a femtosecond laser (Chameleon, 140 fs pulse duration) at fundamental wavelengths of 800 nm, 900 nm, and 1000 nm was focused on the sample by a high numerical aperture microscope objective (NA = 0.95). The SHG emitted by the dimers is collected with the same objective (Figure S4(a) in Supporting Information). We cannot observe the SHG from a gold monomer under the average input power (~ 600 μW) used in the experiment due to the lack of symmetry breaking, as described above.

We measured SHG response of dimers with different degree of asymmetry δ while maintaining excitation at 800 nm wavelength, as shown in Figure 4(a). The color code is the same as before. For different δ, a prominent SHG peak in the spectrum is observed at 400 nm wavelength, accompanied by broad two-photon luminescence (TPL) with comparable intensity. The quadrupole SHG output of the dimer with $\delta = 0$ in our experiments, indicating stronger field gradients in the dimer system. Contrary to our previous expectations, the largest SHG was not observed when δ was the largest.

To understand this behavior, we calculated the near-field enhancement of the electric field in the gap of dimers with different δ. When the particle size is changed, the LBDP resonance of dimers shifts, and respective near-field enhancement at 800 nm changes. It can be seen from Equation 1 that the SHG intensity is proportional to the fourth power of the locally enhanced field inside the dimer gap. We note that the plasmon-induced field enhancement at the double frequency can be ruled out due to the strong contribution of the interband transitions in Au below the ~530 nm wavelength. In Figure 4(b), the histogram shows the SHG intensities of dimers with different δ, while the corresponding calculated fourth power of the electric field enhancement inside the gap at the wavelength of 800 nm is shown with dots. This result is qualitatively consistent with the observation in the experiment: the dimer with $\delta = 0.11$ which exhibits the strongest SHG has the strongest near-field enhancement ($|E_\omega/E_0|^4$) at 800 nm, two orders of magnitude more than the

dimer with δ = 0.14. This also matches the wavelength shift in LBDP resonance. It indicates that the SHG of the dimer originates from the dimer gap and is modulated by the near-field enhancement there under on-resonant excitation.

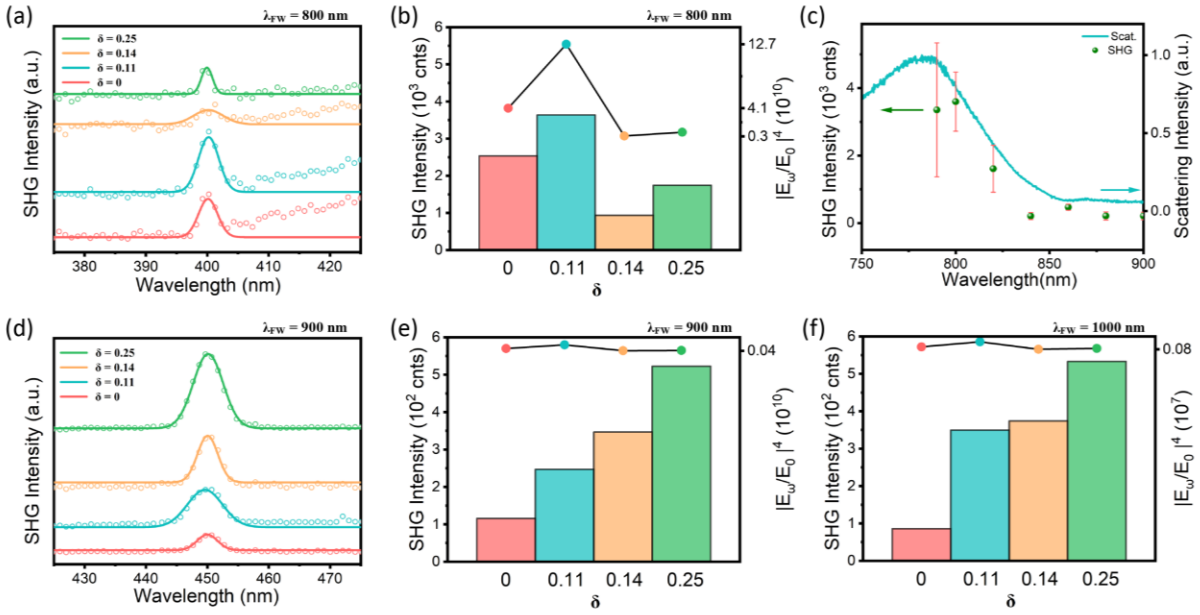

Figure 4: Optical nonlinear properties of dimers with different degrees of asymmetry. (a) SHG spectra of dimers measured (points) and Gaussian fitted (lines) at excitation wavelengths of 800 nm. (b) SHG intensity (histogram, left axis) under on-resonant (λ_{FW} = 800 nm) excitation, which is mainly modulated by the calculated near-field enhancement (dots and line, right axis). (c) Spectra of the SHG measured for the dimer with δ = 0.11 at different excitation wavelengths. Linear scattering spectrum is shown for comparison. (d) SHG spectra of dimers measured (points) and Gaussian fitted (lines) at excitation wavelengths of 900 nm. (e, f) SHG intensity (histogram, left axis) under off-resonant (λ_{FW} = 900 nm, 1000 nm) excitation, which is mainly modulated by symmetry breaking.

To clarify the influence of electric field enhancement in SHG of nanosphere dimer, we also examined the dependence of the SHG intensity on the fundamental wavelength (FW) for a dimer

with $\delta = 0.11$, as shown in Figure 4(c). It can be seen that the strongest SHG was indeed generated at the LBDP resonance (~790 nm) of the dimer with $\delta = 0.11$ where the maximum electric field enhancement is achieved, in good agreement with the prediction based on the numerical simulation. As the wavelength increases, the λ_{FW} moves away from the LDBP resonance, and a rapid decrease in SHG intensity is observed. This indicates that near-field enhancement plays a crucial role in the SHG of gold nanosphere dimer.

However, in the off-resonant case, geometric asymmetry primarily contributes to the SHG of the dimers. In Figure 4(d), the SHG spectra of the dimers excited at $\lambda_{FW} = 900$ nm are presented. It can be seen that as the degree of asymmetry δ increases, the SHG intensity of the dimer also increases. This observation holds true at $\lambda_{FW} = 1000$ nm, which is farther away from the LBDP resonance (see section S1). Under off-resonant conditions, it is worth noting that the near-field enhancement for both configurations is consistently low and in a comparable range (seen in Figure 4(e, f)), which is several orders of magnitude smaller than that under on-resonant case. Therefore, in the case of off-resonant excitation, the SHG enhancement is dominated by symmetry breaking rather than near-field enhancement. Overall, in our experiments, SHG is mainly influenced by two factors: symmetry breaking and plasmon-driven field enhancement. Corresponding to the Equation 1, the first effect changes $\chi^{(2)}$, while the second one changes $E(\omega)$ (local field).

CONCLUSIONS

In conclusion, we demonstrate the modulation of the SHG intensity in gold nanosphere dimers through symmetry breaking. The optical dark field characterization enables us to distinguish monomers and dimers, as well as symmetric and asymmetric dimers, and identify their axis at the single-particle level. Finally, while the near-field enhancement of the gold nanosphere dimers still

dominates the amplification of SHG under on-resonant excitation, we can observe the modulation of SHG intensity due to the symmetry breaking at the off-resonant conditions. Our findings emphasize the significance of symmetry breaking in nonlinear optics and have potential applications in the development of novel nanodevices for optical sensing, imaging, and communication technologies.

ASSOCIATED CONTENT

Supporting Information.

The Supporting Information is available free of charge.

Other results in linear and nonlinear optical characterization, fabrication of samples, and numerical methods.

AUTHOR INFORMATION

Corresponding Author

* Dangyuan Lei - Department of Materials Science and Engineering, City University of Hong Kong, 83 Tat Chee Avenue, Kowloon, Hong Kong S.A.R.; Email: dangylei@cityu.edu.hk

Authors

Yaorong Wang - Department of Materials Science and Engineering, City University of Hong Kong, 83 Tat Chee Avenue, Kowloon, Hong Kong S.A.R.

Zhiwei Peng - Department of Materials Science and Engineering, City University of Hong Kong, 83 Tat Chee Avenue, Kowloon, Hong Kong S.A.R.

Yannick De Wilde - Institut Langevin, ESPCI Paris, CNRS, Université PSL, Paris, 75005 France

Author Contributions

The manuscript was written through contributions of all authors. All authors have given approval to the final version of the manuscript.

Funding Sources

We acknowledge financial support from the Research Grants Council of Hong Kong through a GRF project (11305521) and an ANR/RGC Joint Research Scheme grant (A-CityU101/20) and from LABEX WIFI (Laboratory of Excellence within the French Program Investments for the Future) under references ANR-10-LABX-24 and ANR-10-IDEX-0001-02 PSL* and from the Agence Nationale de la Recherche ANR-20-CE24-0021 “SP-Tunnel-OHG”.

Notes

The authors declare no competing financial interest.

ACKNOWLEDGMENT

Y.W. thanks Dr. Yunxia Wang for her assistance in the initial exploration of SHG experiment, Dr. Meng Qiu, Dr. Ilya Razdolski, Mr. Jiahe Liu for the valuable discussions, and Ms. Xue Ma for the preliminary discussions about dimer assembly.

REFERENCES

(1) You, H.; Li, S.; Fan, Y.; Guo, X.; Lin, Z.; Ding, R.; Cheng, X.; Zhang, H.; Lo, T. W. B.; Hao, J., et al. Accelerated pyro-catalytic hydrogen production enabled by plasmonic local heating of Au on pyroelectric BaTiO3 nanoparticles. *Nat. Commun.* **2022**, 13, 1–9.

(2) Chen, J.; Gong, M.; Fan, Y.; Feng, J.; Han, L.; Xin, H. L.; Cao, M.; Zhang, Q.; Zhang, D.; Lei, D., et al. Collective Plasmon Coupling in Gold Nanoparticle Clusters for Highly Efficient Photothermal Therapy. *ACS nano* **2022**, 16, 910–920.

(3) Shvalya, V.; Vasudevan, A.; Modic, M.; Abutoama, M.; Skubic, C.; Nadižar, N.; Zavašnik, J.; Vengust, D.; Zidanšek, A.; Abdulhalim, I., et al. Bacterial DNA Recognition by SERS Active Plasma-Coupled Nanogold. *Nano Lett.* **2022**, 22 (23), 9757–9765.

(4) Anker, J. N.; Hall, W. P.; Lyandres, O.; Shah, N. C.; Zhao, J.; Van Duyne, R. P. Biosensing with plasmonic nanosensors. *Nat. Mater.* **2008**, 7, 442–453.

(5) Zijlstra, P.; Chon, J. W.; Gu, M. Five-dimensional optical recording mediated by surface plasmons in gold nanorods. *Nature* **2009**, 459, 410–413.

(6) Amendola, V.; Pilot, R.; Frasconi, M.; Maragò, O. M.; Iatì, M. A. Surface plasmon resonance in gold nanoparticles: a review. *J. Phys.: Condens. Matter* **2017**, 29, 203002.

(7) Wang, M.; Wang, T.; Ojambati, O. S.; Duffin, T. J.; Kang, K.; Lee, T.; Scheer, E.; Xiang, D.; Nijhuis, C. A. Plasmonic phenomena in molecular junctions: Principles and applications. *Nat. Rev. Chem.* **2022**, 6, 681–704.

(8) Zohar, N.; Chuntonov, L.; Haran, G. The simplest plasmonic molecules: Metal nanoparticle dimers and trimers. *J. Photochem. Photobiol., C* **2014**, 21, 26–39.

(9) Ahmadivand, A.; Semmlinger, M.; Dong, L.; Gerislioglu, B.; Nordlander, P.; Halas, N. J. Toroidal dipole-enhanced third harmonic generation of deep ultraviolet light using plasmonic meta-atoms. *Nano Lett.* **2018**, 19, 605–611.

(10) Cha, H.; Yoon, J. H.; Yoon, S. Probing quantum plasmon coupling using gold nanoparticle dimers with tunable interparticle distances down to the subnanometer range. *ACS nano* **2014**, 8, 8554–8563.

(11) Tan, S. F. *Molecular Electronic Control Over Tunneling Charge Transfer Plasmons Modes*; Springer, **2018**.

(12) Camargo, P. H.; Rycenga, M.; Au, L.; Xia, Y. Isolating and probing the hot spot formed between two silver nanocubes. *Angew. Chem., Int. Ed.* **2009**, 121, 2214–2218.

(13) Lim, D.-K.; Jeon, K.-S.; Kim, H. M.; Nam, J.-M.; Suh, Y. D. Nanogap-engineerable Raman-active nanodumbbells for single-molecule detection. *Nat. Mater.* **2010**, 9, 60–67.

(14) Zhang, Z.; Deckert-Gaudig, T.; Singh, P.; Deckert, V. Single molecule level plasmonic catalysis–a dilution study of p-nitrothiophenol on gold dimers. *Chem. Commun.* **2015**, 51, 3069–3072.

(15) Zhang, C.; Zhao, H.; Zhou, L.; Schlather, A. E.; Dong, L.; McClain, M. J.; Swearer, D. F.; Nordlander, P.; Halas, N. J. Al–Pd nanodisk heterodimers as antenna– reactor photocatalysts. *Nano Lett.* **2016**, 16, 6677–6682.

(16) Slablab, A.; Le Xuan, L.; Zielinski, M.; De Wilde, Y.; Jacques, V.; Chauvat, D.; Roch, J.-F. Second-harmonic generation from coupled plasmon modes in a single dimer of gold nanospheres. *Opt. Express* **2012**, 20, 220–227.

(17) Franken, P.; Hill, A. E.; Peters, C. e.; Weinreich, G. Generation of optical harmonics. *Phys. Rev. Lett.* **1961**, 7, 118.

(18) Butet, J.; Brevet, P.-F.; Martin, O. J. Optical second harmonic generation in plasmonic nanostructures: from fundamental principles to advanced applications. *ACS nano* **2015**, 9, 10545–10562.

(19) Butet, J.; Duboisset, J.; Bachelier, G.; Russier-Antoine, I.; Benichou, E.; Jonin, C.; Brevet, P.-F. Optical second harmonic generation of single metallic nanoparticles embedded in a homogeneous medium. *Nano Lett.* **2010**, 10, 1717–1721.

(20) Butet, J.; Bachelier, G.; Russier-Antoine, I.; Jonin, C.; Benichou, E.; Brevet, P.-F. Interference between selected dipoles and octupoles in the optical second-harmonic generation from spherical gold nanoparticles. *Phys. Rev. Lett.* **2010**, 105, 077401.

(21) Nappa, J.; Revillod, G.; Russier-Antoine, I.; Benichou, E.; Jonin, C.; Brevet, P. Electric dipole origin of the second harmonic generation of small metallic particles. *Phys. Rev. B* **2005**, 71, 165407.

(22) Nappa, J.; Russier-Antoine, I.; Benichou, E.; Jonin, C.; Brevet, P. Second harmonic generation from small gold metallic particles: from the dipolar to the quadrupolar response. *J. Chem. Phys.* **2006**, 125, 184712.

(23) Meier, J.; Zurak, L.; Locatelli, A.; Feichtner, T.; Kullock, R.; Hecht, B. Controlling field asymmetry in nanoscale gaps for second harmonic generation. Advanced Optical Materials **2023**. 2300731.

(24) Johnson, J. C.; Yan, H.; Schaller, R. D.; Petersen, P. B.; Yang, P.; Saykally, R. J. Nearfield imaging of nonlinear optical mixing in single zinc oxide nanowires. *Nano Lett.* **2002**, 2, 279–283.

(25) Nakayama, Y.; Pauzauskie, P. J.; Radenovic, A.; Onorato, R. M.; Saykally, R. J.; Liphardt, J.; Yang, P. Tunable nanowire nonlinear optical probe. *Nature* **2007**, 447, 1098–1101.

(26) O'Brien, K.; Suchowski, H.; Rho, J.; Salandrino, A.; Kante, B.; Yin, X.; Zhang, X. Predicting nonlinear properties of metamaterials from the linear response. *Nat. Mater.* **2015**, 14, 379–383.

(27) Neely, A.; Perry, C.; Varisli, B.; Singh, A. K.; Arbneshi, T.; Senapati, D.; Kalluri, J. R.; Ray, P. C. Ultrasensitive and highly selective detection of Alzheimer's disease biomarker using two-photon Rayleigh scattering properties of gold nanoparticle. *ACS nano* **2009**, 3, 2834–2840.

(28) Li, G.-C.; Zhang, Y.-L.; Jiang, J.; Luo, Y.; Lei, D. Y. Metal-substrate-mediated plasmon hybridization in a nanoparticle dimer for photoluminescence line-width shrinking and intensity enhancement. *ACS nano* **2017**, 11, 3067–3080.

(29) Canfield, B. K.; Kujala, S.; Jefimovs, K.; Turunen, J.; Kauranen, M. Linear and nonlinear optical responses influenced by broken symmetry in an array of gold nanoparticles. *Opt. Express* **2004**, 12, 5418–5423.

(30) Husu, H.; Canfield, B. K.; Laukkanen, J.; Bai, B.; Kuittinen, M.; Turunen, J.; Kauranen, M. Local-field effects in the nonlinear optical response of metamaterials. *Metamaterials* **2008**, 2, 155–168.

(31) Canfield, B. K.; Husu, H.; Laukkanen, J.; Bai, B.; Kuittinen, M.; Turunen, J.; Kauranen, M. Local Field Asymmetry Drives Second-Harmonic Generation in Noncentrosymmetric Nanodimers. *Nano Lett.* **2007**, 7, 1251–1255.

(32) Kravets, V. G.; Kabashin, A. V.; Barnes, W. L.; Grigorenko, A. N. Plasmonic Surface Lattice Resonances: A Review of Properties and Applications. *Chem. Rev.* **2018**, 118, 5912–5951.

(33) Yoon, J. H.; Selbach, F.; Langolf, L.; Schlücker, S. Ideal Dimers of Gold Nanospheres for Precision Plasmonics: Synthesis and Characterization at the Single-Particle Level for Identification of Higher Order Modes. *Small* **2018**, 14, 1702754.

(34) Heuer-Jungemann, A.; Feliu, N.; Bakaimi, I.; Hamaly, M.; Alkilany, A.; Chakraborty, I.; Masood, A.; Casula, M. F.; Kostopoulou, A.; Oh, E., et al. The role of ligands in the chemical synthesis and applications of inorganic nanoparticles. *Chem. Rev.* **2019**, 119, 4819–4880.

(35) Jose, J.; Schumacher, L.; Jalali, M.; Haberfehlner, G.; Svejda, J. T.; Erni, D.; Schlücker, S. Particle Size-Dependent Onset of the Tunneling Regime in Ideal Dimers of Gold Nanospheres. *ACS nano* **2022**, 16 (12), 21377–21387.

(36) Yang, L.; Wang, H.; Fang, Y.; Li, Z. Polarization state of light scattered from quantum plasmonic dimer antennas. *ACS nano* **2016**, 10, 1580–1588.

(37) Yoon, J. H.; Selbach, F.; Schumacher, L.; Jose, J.; Schlücker, S. Surface plasmon coupling in dimers of gold nanoparticles: Experiment and theory for ideal (spherical) and nonideal (faceted) building blocks. *ACS Photonics* **2019**, 6, 642–648.

(38) Prodan, E.; Radloff, C.; Halas, N. J.; Nordlander, P. A hybridization model for the plasmon response of complex nanostructures. *Science* **2003**, 302, 419–422.

(39) Nordlander, P.; Oubre, C.; Prodan, E.; Li, K.; Stockman, M. Plasmon hybridization in nanoparticle dimers. *Nano lett.* **2004**, 4, 899–903.

(40) Jain, P. K.; Eustis, S.; El-Sayed, M. A. Plasmon coupling in nanorod assemblies: optical absorption, discrete dipole approximation simulation, and exciton-coupling model. *J. Phys. Chem. B* **2006**, 110, 18243–18253.

(41) Thomas, K. G.; Barazzouk, S.; Ipe, B. I.; Joseph, S. S.; Kamat, P. V. Uniaxial plasmon coupling through longitudinal self-assembly of gold nanorods. *J. Phys. Chem. B* **2004**, 108, 13066–13068.

(42) Abou-Hamdan, L.; Li, C.; Haidar, R.; Krachmalnicoff, V.; Bouchon, P.; De Wilde, Y. Hybrid modes in a single thermally excited asymmetric dimer antenna. *Opt. Lett.* **2021**, 46, 981–984.

(43) Ha, J. W. Characteristic image patterns of single anisotropic plasmonic nanoparticles embedded in a gel matrix. *Nanoscale* **2015**, 7, 13159–13163.

(44) Zhang, Q.; Li, G.; Lo, T.; Lei, D. Polarization-resolved optical response of plasmonic particle-on-film nanocavities. *Journal of Optics* **2018**, 20, 024010.

(45) Ulman, A. Formation and structure of self-assembled monolayers. *Chem. Rev.* **1996**, 96, 1533–1554.

(46) Widrig, C. A.; Chung, C.; Porter, M. D. The electrochemical desorption of n-alkanethiol monolayers from polycrystalline Au and Ag electrodes. *J. Electroanal. Chem.* **1991**, 310, 335–359.

(47) Slowinski, K.; Chamberlain, R. V.; Bilewicz, R.; Majda, M. Evidence for inefficient chain-to-chain coupling in electron tunneling through liquid alkanethiol monolayer films on mercury. *J. Am. Chem. Soc.* **1996**, 118, 4709–4710.

(48) Miller, C.; Cuendet, P.; Graetzel, M. Adsorbed. omega.-hydroxy thiol monolayers on gold electrodes: evidence for electron tunneling to redox species in solution. *J. Phys. Chem.* **1991**, 95, 877–886.

(49) Porter, M. D.; Bright, T. B.; Allara, D. L.; Chidsey, C. E. Spontaneously organized molecular assemblies. 4. Structural characterization of n-alkyl thiol monolayers on gold by optical ellipsometry, infrared spectroscopy, and electrochemistry. *J. Am. Chem. Soc.* **1987**, 109, 3559–3568.

(50) Krasavin, A. V.; Ginzburg, P.; Zayats, A. V. Free-electron optical nonlinearities in plasmonic nanostructures: a review of the hydrodynamic description. *Laser Photonics Rev.* **2018**, 12, 1700082.

(51) Berthelot, J.; Bachelier, G.; Song, M.; Rai, P.; Des Francs, G. C.; Dereux, A.; Bouhelier, A. Silencing and enhancement of second-harmonic generation in optical gap antennas. *Opt. Express* **2012**, 20, 10498–10508.

TOC Graphic

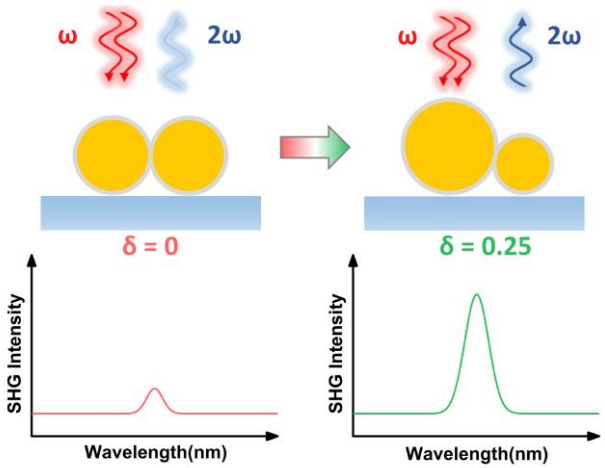
ω
2ω
δ = 0
SHG Intensity
Wavelength(nm)
ω
2ω
δ = 0.25
SHG Intensity
Wavelength(nm)

Supporting Information

Symmetry Breaking-induced Enhancement of Second Harmonic Generation in Gold Nanosphere Dimers

Yaorong Wang,[†] Zhiwei Peng,[†] Danjun Liu,[†] Yannick De Wilde,[‡] and Dangyuan Lei[,†]*

[†]Department of Materials Science and Engineering, City University of Hong Kong, 83 Tat Chee Avenue, Kowloon, Hong Kong S.A.R., China

[‡] Institut Langevin, ESPCI Paris, CNRS, Université PSL, Paris, 75005 France

*E-mail: dangylei@cityu.edu.hk

Content

1. Sample fabrication

Highly spherical gold nanoparticles (NanoSeedz) of varying diameters (~60 nm, ~80 nm, and ~100 nm) were sequentially assembled on a substrate to prepare dimers. The gold nanosphere were coated with a surfactant layer of cetyltrimethylammonium bromide (CTAB). As shown in Figure S1(a), the synthesis of the dimers comprises five steps.

Step 1: The starting materials for the dimers are CTAB-capped gold nanoparticles and cleaned glass. A glass slide (25 mm × 12 mm) cleaned with a hot RBS detergent solution (15%, 90 °C) was immersed in a CTAB solution (5×10^{-6} m, 5 mL) containing gold nanoparticles (5×10^{-12} m) for 17 h at 30 °C. All subsequent steps were performed at 30 °C. The glass substrate was given a negative charge by washing them in RBS detergent solution. The surface charge of nanoparticles is mainly regulated by surface ligands: the common positive charge ligands like CTAB and negatively charged ligands like polyvinylpyrrolidone (PVP). But in different solvents, the surface electrical properties of nanoparticles with the same surface ligands can be significantly modified. For example, CTAB-capped gold exhibits positive electrical properties in aqueous solution, but significantly negative electrical properties in acetonitrile solution. In this step, the first nanoparticle is made to attach to the glass substrate via the electrostatic interaction between the substrate and the positively charged CTAB bilayer surrounding the nanoparticle. We refer to the gold nanoparticles as the first and second nanoparticle according to the order in which they were added to the system.

Step 2: The glass slide was washed with water and ethanol (ACS grade, Anaqua). For a well-ordered linker self-assembled monolayer (SAM) on the surface of the nanoparticles, the washed glass was exposed to a mixture of an ethanolic solution of the 1,8 octanedithiol (C8, ≥ 98%, Aladdin) and an aqueous solution of sodium bromide (NaBr, ≥ 99%, Aladdin)(v/v 250:1). The final concentration of both alkanedithiol and NaBr was 1×10^{-3} m. The addition of inorganic salts to the aqueous suspension medium such as NaBr or the use of organic suspension media such as acetonitrile increases the critical micelle concentration of CTAB on the metal surface.[1,2]

Importantly, only the combination of both inorganic salt and organic suspension medium efficiently destroys the CTAB bilayer, so that a well-ordered linker SAM forms within 1 h.

Step 3: The glass substrate coated with the nanoparticles was washed using ethanol. For the synthesis of the dimers, the glass slide was dipped into 5 mL of acetonitrile (HPLC grade, RciLabscan) containing nanoparticles (20×10^{-12} m) and NaBr (200×10^{-6} m) for 5 h. If an asymmetric dimer has to be prepared, gold spheres with larger diameters need to be added at this step.

Step 4: For stabilizing the surface of the secondly added nanoparticles, the glass substrate was washed using ethanol and immersed for 1 h in a mixture of an ethanolic solution of (11-mercaptoundecyl)-N,N,N-trimethylammonium bromide (MUTAB, ≥ 90%, Aldrich) and an aqueous solution of NaBr (v/v 250:1). The final concentration of MUTAB is 1×10^{-3} m.

Step 5: Dimers were removed from the glass substrate using sonication for 30 s. For the stabilization of the newly exposed area of ideal dimers upon the sonication, an ethanolic solution of MUTAB (10×10^{-6} m) was employed as a dispersion medium.

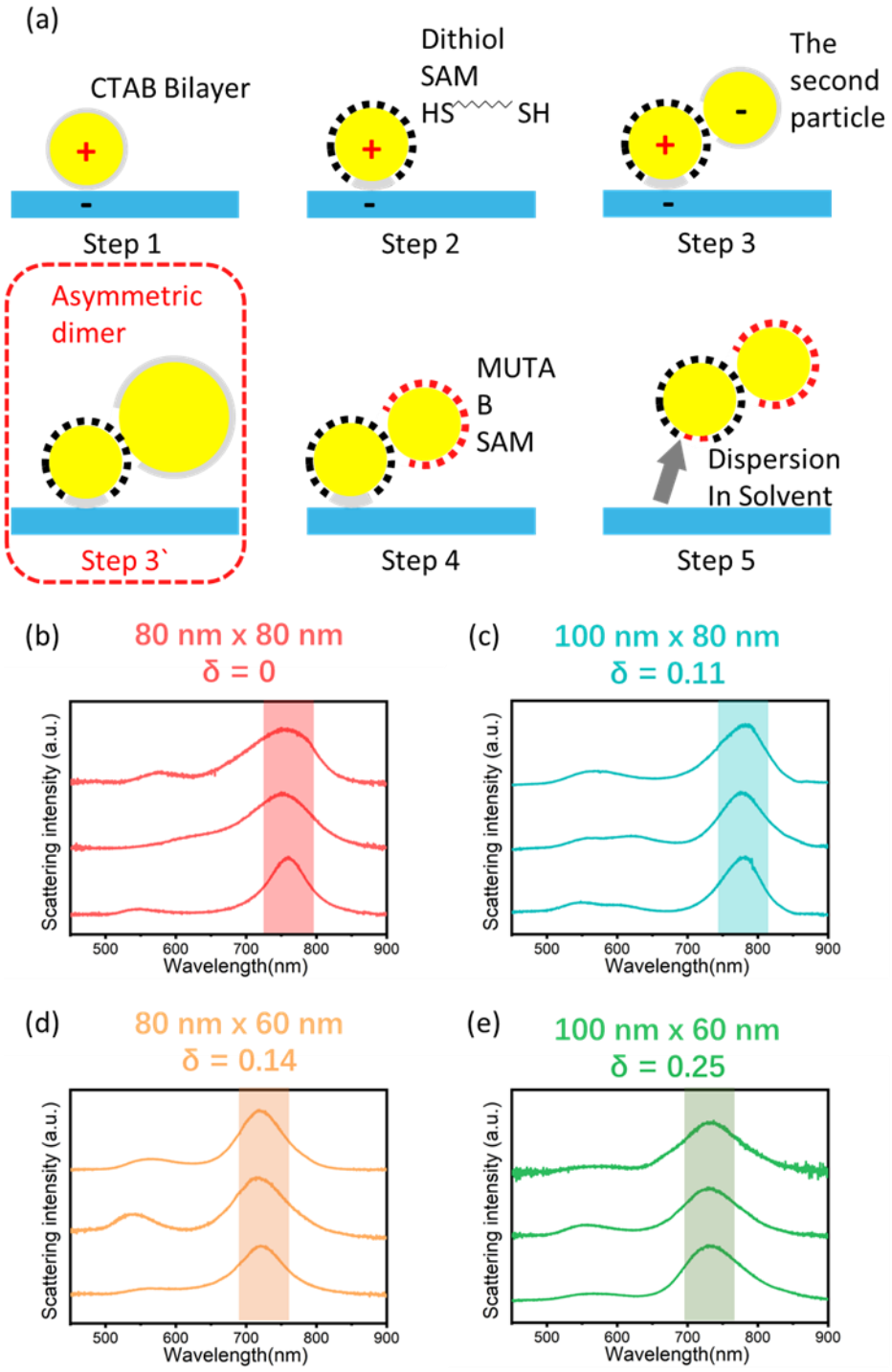

Figure S1. (a) Schematic diagram of the assembled dimer. Single-particle dark-field scattering spectra of b) 80 x 80 nm dimers, c) 100 x 80 nm dimers, d) 80 x 60 nm dimers, e),100 x 60 nm dimers. The LBDP band is highlighted.

2.Numerical methods for SHG simulations

In the nonlinear simulations, we adopted the perturbative approach within the undepleted pump approximation, which is justified by the fact that the SHG field intensity generated by a plasmonic nanostructure is always orders of magnitude weaker than that of the excitation field. Under this approximation, the SHG field does not couple back to the pump field and, therefore, the nonlinear process can be decomposed into two linear scattering processes: firstly, the fundamental fields were solved with the finite element solver in the frequency domain and the calculated fields were used to find the SHG polarization source currents that are responsible for the far-field SHG emission. Although both the free and bound electrons in metals can give rise to the second-order nonlinear process, it has been proven that only the former is responsible for the dominant SHG response in the visible and near- infrared spectral range.[3] The SHG polarization currents related to free electrons can be further decomposed into the volume and surface contributions. Here, we only consider the second-harmonic polarization which is normal to the metal surface for it plays the dominant role in the SHG.[4,5] In this case, the SHG source currents based on the free-electron hydrodynamic model can be found as[5]

$$\hat{\mathbf{n}} \cdot \mathbf{J}_{\mathrm{surf}} = i \frac{n_0 e^3}{2m_*^2} \frac{3+\varepsilon_{\mathrm{EF}}(\omega)}{(\omega+i\gamma)^2(2\omega+i\gamma)} E_\perp^2(\omega) \tag{1}$$

where $\hat{\mathbf{n}}$ is the unit vector normal to the metal surface, $\mathbf{J}_{\mathrm{surf}}$ is the surface current, n_0 is the free-electron density in gold, m_* represents the effective electron mass, e is the elementary charge, γ is the electron gas collision frequency in gold, $\varepsilon_{\mathrm{EF}}$ is the bulk gold permittivity at the fundamental wavelength, and $E_\perp(\omega)$ is the normal component of the local fundamental field at the metal surface. Due to the limited penetration of the electromagnetic fields into the bulk gold, the induced nonlinear polarization occurs mainly in the sub-nanometer-thick surface layer. Considering the rotational symmetry of a nanoparticle dimer, the simulation configuration can be simplified into a two-dimensional frame for which the meshing for the surface layer, where the SHG source is located, can be scaled down to the level of 0.1 Å (Figure S2).

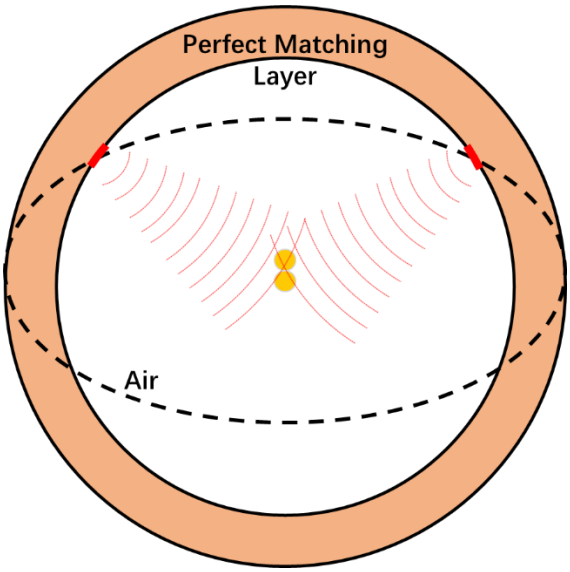

Figure S2 Simulation domains for a gold nanoparticle dimer. The excitation source is modeled by the current oscillator with the oscillation direction tangential to the inner surface of the perfectly matching layer. Such excitation configuration can preferentially excite the gap plasmon modes of the gold nanoparticle dimer.

3. Linear optical properties of dimers

Optical microscopy and spectroscopy were performed with an Olympus microscope equipped with a standard dark-field optical module using a 100× dark-field objective (LMPlanFLN, Olympus, NA=0.8). Dark-field images and the spectra of individual nanostructures were recorded respectively using a color CCD camera (OPLENIC) and a spectrograph (Andor SR500i). The individual nanosphere monomers and dimers on a silica substrate show significantly different scattering responses. These distinct properties can thus be employed to identify the nanoparticle dimers from the monomers and to determine their in-plane orientations with the polarization-resolved dark-field microscopy.

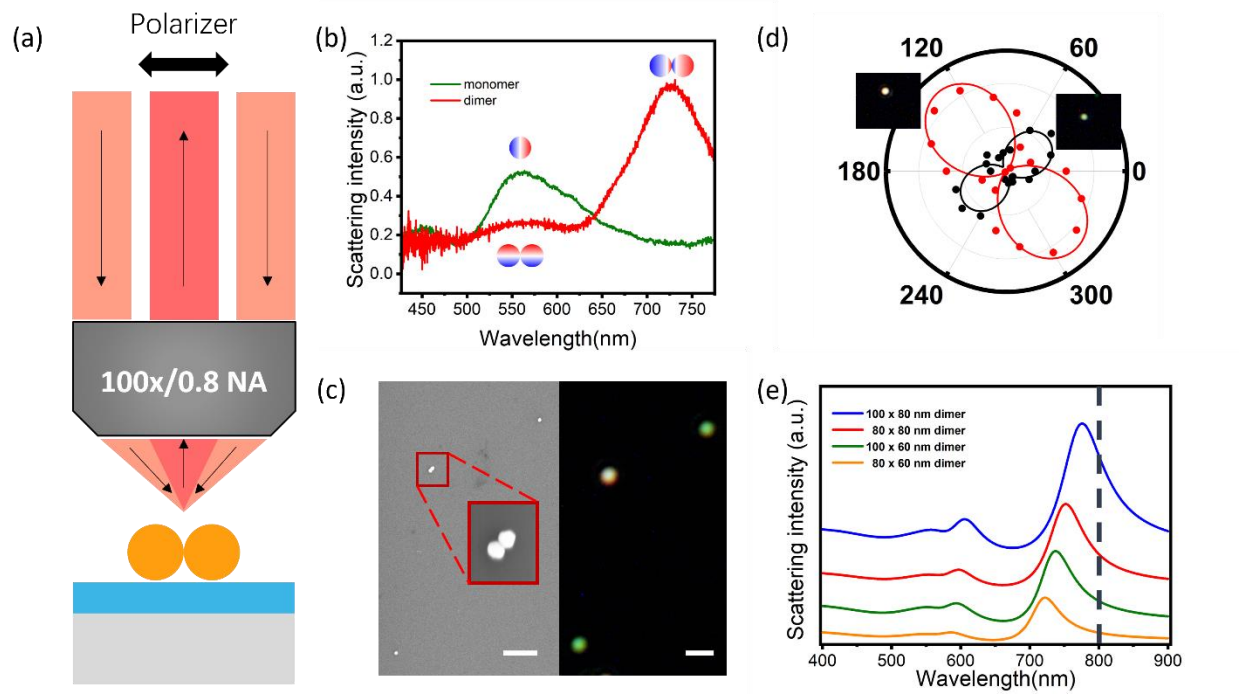

Figure S3 (a) Experimental schematic for DF. (b) Scattering spectrum of a gold nanoparticle monomer and dimer on the substrate. Insets show the diagram of their modes. (c) SEM micrograph (left) of two nanosphere monomers and a nanosphere dimer (enclosed by the red square). The right panel shows the corresponding optical dark-field image for the same sample area. The scale bars in both images are 1 μm. (d) The dimer exhibits polarization-dependent scattering intensity patterns, which can be employed to determine its orientation. The inset shows DF images with different polarization orientations. (e) Simulated scattering spectra of different dimers.

4. Experimental setup for nonlinear optical spectroscopy and power dependence of the SHG

A Ti: sapphire femtosecond laser (Chameleon, pulse duration ~140 fs, repetition frequency 80 MHz) delivers laser pulses into an inverted microscope (MPlanApo 480 100x, Olympus, NA=0.95). Polarizer inserted into the beam path fixes the polarization state of the laser beam, and the axis of the dimer is also fixed in the same direction. This is because we can know the axis of the dimer by DF, as described earlier. The SHG signal from gold dimers in the focal plane is collected by the same objective, and then reflected into the detection path by two beam splitters

(BS). A 600 nm short-pass filter was inserted in the detection path, which removed the pump laser and allowed the SHG signal to pass. And certain TPL signals are filtered out as well. Please note that the objective lens, BS, and filter used in our experimental system have different transmittances for different wavelengths in the visible range. We unify the power of the 800 nm, 900 nm, and 1000 nm lasers after being focused by the objective lens. The transmittance of the whole system to 400 nm, 450 nm, and 500 nm are about 6%, 26%, and 23% respectively.

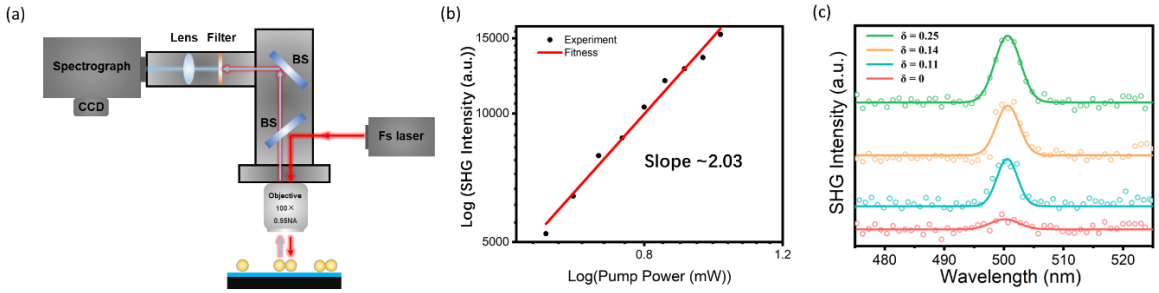

Figure S4 (a) Experimental setup for nonlinear optical spectroscopy. (b) The pump-power dependence of the SHG. (c) SHG spectra of dimers measured (points) and Gaussian fitted (lines) at excitation wavelengths of 1000 nm.

5. Evaluation of laser damage to the gold nanoparticle dimers

Since the gap plasmon resonance of dimer is sensitive to the gap morphology and distance, we rely on the comparison of the measured scattering spectra of single nanostructures before and after the laser irradiation. For the laser irradiation power ~0.6 mW, most of the nanoparticle dimers show scattering spectra as in Figure S5. The peak shift of less than 10 nm indicates negligible gap variation. In our experiments, the peak intensity of a single pulse is about 5 GW/cm^2, and the duration of each measurement is 90 s.

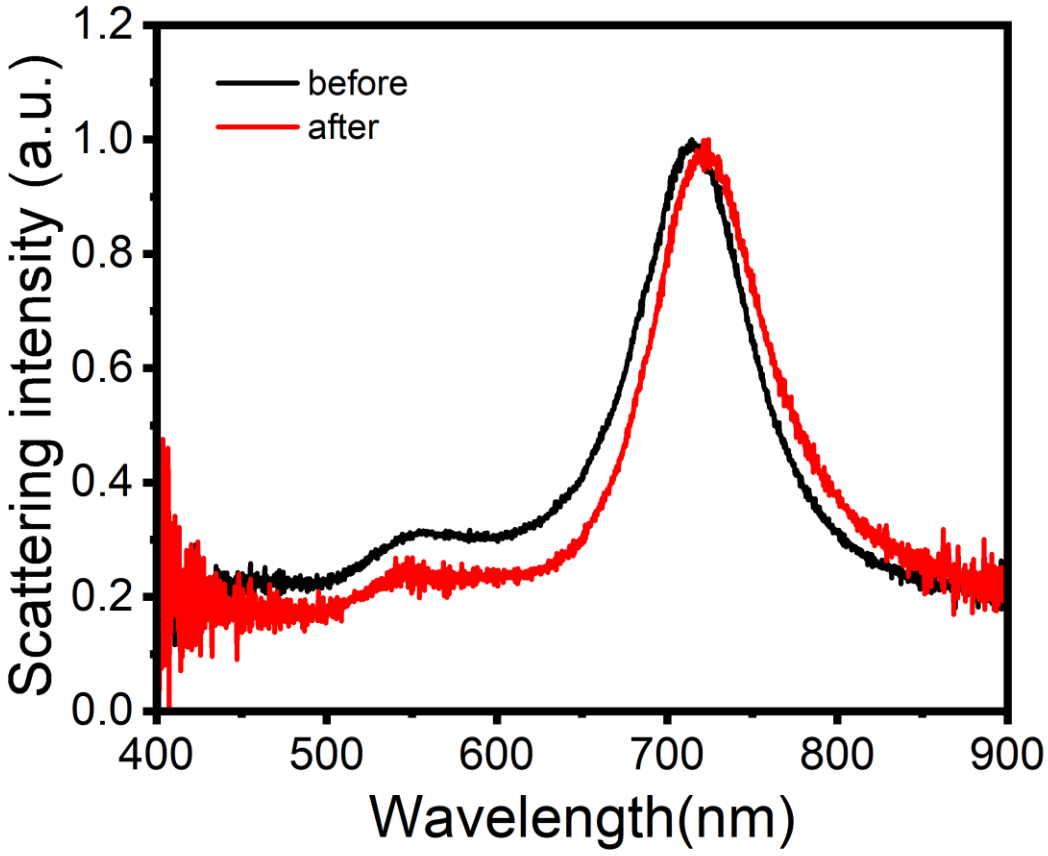

Figure S5 Representative scattering spectra of a nanoparticle dimer measured before and after the SHG measurements.

References

(1) Liu, K.; Zheng, Y.; Lu, X.; Thai, T.; Lee, N. A.; Bach, U.; Gooding, J. J. Biocompatible gold nanorods: One-step surface functionalization, highly colloidal stability, and low cytotoxicity. *Langmuir* 2015, *31*, 4973–4980.

(2) Nepal, D.; Park, K.; Vaia, R. A. High-Yield Assembly of Soluble and Stable Gold Nanorod Pairs for High-Temperature Plasmonics. *Small* 2012, *8*, 1013–1020.

(3) Scalora, M.; Vincenti, M. A.; de Ceglia, D.; Roppo, V.; Centini, M.; Akozbek, N.; Bloemer, M. Second-and third-harmonic generation in metal-based structures. *Physical Review A* 2010, *82*, 043828.

(4) Krasavin, A. V.; Ginzburg, P.; Zayats, A. V. Free-electron optical nonlinearities in plasmonic nanostructures: a review of the hydrodynamic description. *Laser & Photonics Reviews* 2018, *12*, 1700082.

(5) Marino, G.; Segovia, P.; Krasavin, A. V.; Ginzburg, P.; Olivier, N.; Wurtz, G. A.; Zayats, A. V. Second-harmonic generation from hyperbolic plasmonic nanorod metamaterial slab. *Laser & Photonics Reviews* 2018, *12*, 1700189.